Acta Cryst. (1997). B**53**, 861–869

Structure Refinements of the Layered Intergrowth Phases $Sb^{III}Sb^{V}_{x}A_{1-x}TiO_6$ ($x \simeq 0$, A = Ta, Nb) Using Synchrotron X-ray Powder Diffraction Data

CHRISTOPHER D. LING,[a]* JOHN G. THOMPSON,[a] SIEGBERT SCHMID,[a] DAVID J. COOKSON[b] AND RAY L. WITHERS[a]

[a]*Research School of Chemistry, Australian National University, Canberra ACT 0200, Australia, and* [b]*Australian National Beamline Facility, ANSTO, Menai 2234, Australia. E-mail: ling@rsc.anu.edu.au*

(*Received 3 January 1997; accepted 23 May 1997*)

Abstract

The structures of the layered intergrowth phases $Sb^{III}Sb^{V}_{x}A_{1-x}TiO_6$ ($x \simeq 0$, A = Ta, Nb) have been refined by the Rietveld method, using X-ray diffraction data obtained using a synchrotron source. The starting models for these structures were derived from those of $Sb^{III}_{3}Sb^{V}_{x}A_{3-x}TiO_{14}$ (x = 1.26, A = Ta and x = 0.89, A = Nb), previously solved by single crystal X-ray diffraction. There were no significant differences between the derived models and the final structures, validating the approach used to obtain the models and confirming that the n = 1 and n = 3 members of the family $Sb^{III}_{n}Sb^{V}_{x}A_{n-x}TiO_{4n+2}$ are part of a structurally homologous series.

1. Introduction

Many complex layered phases, consisting of ordered intergrowths of slabs of simpler structure types, are known. The archetypal example is the bismuth oxide-based family of Aurivillius phases (Aurivillius, 1949), based on a parent structure consisting of perovskite-like $A_{n-1}B_nO_{3n+1}$ slabs regularly interleaved with α-PbO-type $Bi_2O_2^{2+}$ layers. In a recent investigation into antimony-based analogues of these bismuth-based phases (Ling, Thompson, Withers & Schmid, 1996), two new phases were discovered with approximate compositions $SbATiO_6$ (A = Nb, Ta). Further investigation of these ternary oxide systems revealed that the initially discovered phases were members of a compositional series $Sb^{III}_{n}Sb^{V}_{x}A_{n-x}TiO_{4n+2}$, the observed members being n = 1, 3 (A = Nb) and n = 1, 2, 3 (A = Ta). The presence of Sb^{V} in the formula was deduced from variable Sb:A ratios measured by energy-dispersive X-ray analysis (EDAX) in a scanning electron microscope (SEM) from within ostensibly single crystal domains (*e.g.* for $Sb^{III}_{3}Sb^{V}_{x}Ta_{3-x}TiO_{14}$, $0.7 \leq x \leq 1.8$). Despite this micron-scale compositional variation the XRD profiles for these phases showed no significant peak broadening, suggesting that Sb^{V} could substitute for A^{V} to form a solid solution with little change in unit-cell dimensions.

The similarity of the general formula $Sb^{III}_{n}Sb^{V}_{x}A_{n-x}TiO_{4n+2}$ to that of the Aurivillius phases $Bi_2O_2.A_{n-1}B_nO_{3n+1}$ suggested the former might also be a homologous series of layered intergrowth phases. Electron diffraction (ED) investigations (Ling, Thompson *et al.*, 1996) strongly supported this hypothesis, indicating that n = 1, 2 and 3 were layered structures with the same average metal-atom layer spacing of ~2.8 Å, comprising 6, 10 and 14 metal-atom layer repeats, respectively. In order to determine the structures of the observed members and test the hypothesis, attempts were made to grow single crystals. The only crystals successfully grown, however, were n = 3; n = 1 could only be obtained as a powder and n = 2 (A = Ta) was always observed as an intergrowth in n = 3 crystals. Two crystal structures were subsequently solved and refined; $Sb^{III}_{3}Sb^{V}_{x}Nb_{3-x}TiO_{14}$, x = 0.89, and $Sb^{III}_{3}Sb^{V}_{x}Ta_{3-x}TiO_{14}$, x = 1.26 (Ling, Schmid, Thompson, Withers & Sterns, 1996). These n = 3 phases possess isomorphous layered structures based on the intergrowth of units with α-Sb_2O_3-type and Sb_2O_5-type structures (Hyde & Andersson, 1989).

The models for the n = 1 and n = 2 members of the series used the same basic structural elements observed in the n = 3 structure (Ling, Thompson *et al.*, 1996), while complying with the symmetry and compositional constraints provided by X-ray diffraction (XRD), ED and EDAX data. In particular, the space-group symmetries, determined by ED, led to unambiguous models, assuming the same basic structural elements were present in all members of the series. The models were shown to be chemically plausible by the empirical calculation of bond-valence sums (Brese & O'Keefe, 1991). Single phase powders obtained for the n = 1 phases allowed comparison of observed XRD patterns to those calculated from the models and the qualitative match observed indicated that the models were approximately correct. Attempts to refine the structures using the Rietveld method were, however, limited by the resolution of the data which could be obtained using conventional X-ray sources. Only unit-cell parameters and metal-atom positions could be refined without causing the refinements to diverge. Although refinement of these parameters supported the models, they hardly constituted a satisfactory structure solution.

Full refinements of the proposed n = 1 models were necessary in order to properly compare the n = 1 and

$n = 3$ members of the series, and the A = Nb and A = Ta forms of $n = 1$, confirming that the new layered phases formed an homologous series. To obtain the best possible structure refinements from XRD using the Rietveld method, it was advisable to utilize a synchrotron X-ray source. The higher resolution would reduce peak overlap at high angles, allowing refinement of a greater number of reflections, as well as improving peak profiles throughout the pattern. Synchrotron data offered the added bonus of smaller sample sizes (making it easier to obtain single-phase specimens) and tunable energies, which it was hoped would assist in discriminating metal atoms and hence refining the compositions of the mixed sites in the models.

2. Synthesis and characterization

Single-phase powders of $Sb^{III}Sb_x^VNb_{1-x}TiO_6$ were synthesized by the solid-state reaction of a mixture of Sb_2O_3 (Aldrich 99.99%), Nb_2O_5 (Koch-Lite 99.9%) and TiO_2 (Halewood 99.998%), heated in the molar ratio 1.2:0.9:1, in a sealed platinum tube, to 1073 K for 2 h, then 1273 K for 3 h, then 1373 K for 16 h. An homogeneous pale-yellow powder was obtained. Single-phase powders of $Sb^{III}Sb_x^VTa_{1-x}TiO_6$ were synthesized in the same fashion (Aldrich 99.99% Ta_2O_5). Both powders were identified as predominantly single phase by XRD using a Guinier–Hägg camera with conventional (Cu $K\alpha_1$) radiation.

The compositions of the samples were investigated using a Jeol 6400 SEM equipped with a Link ATW detector. Quantitative energy-dispersive spectroscopic (EDS) analyses were made at 15 kV and 1 nA with data processed using the Link ISIS system. ZAF (atomic number/absorption/fluorescence) corrections were made using the *SEM-QUANT* software package (Oxford Instruments ISIS System). $TiNb_2O_7$, Ta_2O_5 and Sb metal were used as analytical standards for Ti, Nb, Ta and Sb, respectively. Sintered polycrystalline samples were embedded in epoxy resin and diamond polished to a 1 mm finish to facilitate quantitative microanalysis.

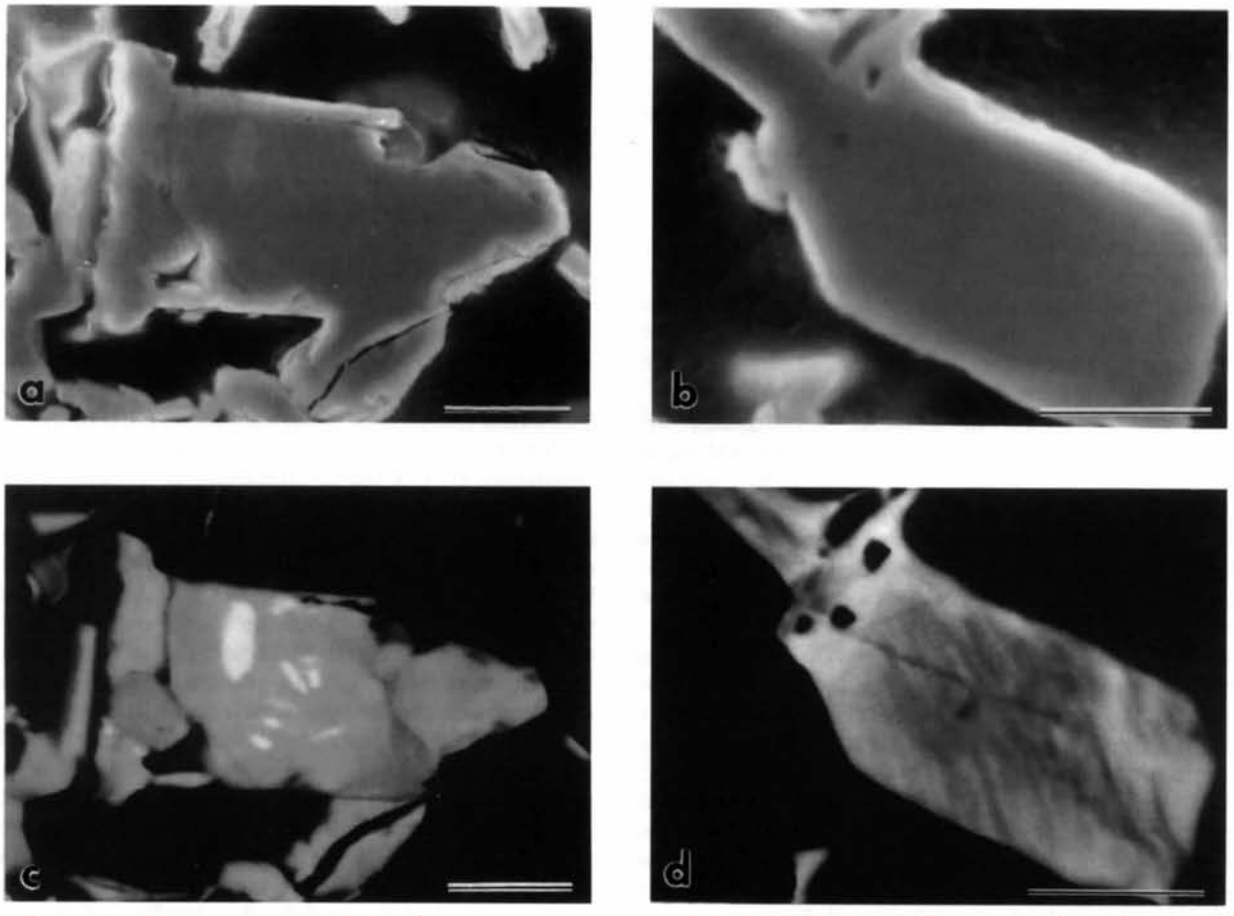

Fig. 1. Scanning electron micrographs of polished cross sections of powder samples embedded in epoxy resin. Secondary electron images are at the top (*a*, *b*) with backscattered electron images below (*c*, *d*); left-hand images (*a*, *c*) are of $Sb^{III}Sb_x^VTa_{1-x}TiO_6$ and right-hand images (*b*, *d*) are of $Sb^{III}Sb_x^VNb_{1-x}TiO_6$. Scale bars are 5 mm in each case. The crystals in the backscattered electron images appear smaller than the corresponding secondary electron images, as the rounded edges due to polishing show up black.

Microanalysis of the two powder specimens used for XRD data collection provided somewhat surprising results, given that the synchrotron XRD data showed that the tantalate specimen contained a single crystalline phase and the niobate specimen a minor crystalline impurity, $TiNb_2O_7$. For both specimens spot analyses from larger crystals and crystalline aggregates gave quite variable compositions, while analyses from edge-on 2–3 mm thick plates gave metal compositions of $Sb_{1.10\,(5)}A_{0.90\,(5)}Ti_{1.00\,(5)}$, consistent with the starting composition of $Sb_{1.2}A_{0.9}Ti_{1.0}$, which included 9% excess Sb_2O_3 to help flux the crystal growth.

Fig. 1 shows backscattered electron images (*c* and *d*) juxtaposed to secondary electron images (*a* and *b*) from the same areas of the embedded polycrystalline specimens for both samples. The backscattered electron images show a rather dramatic variation in composition on the micron to sub-micron scale for both the tantalate and the niobate specimens. In the tantalate specimen (Fig. 1*c*) the light spots (higher average atomic number) and the dark regions (lower average atomic number) are depleted and enriched, respectively, in titanium relative to the expected composition while the Sb:Ta ratio remains approximately constant. In the niobate specimen (Fig. 1*d*) only titanium depletion (the dark bands) was observed.

One explanation for the micron to sub-micron scale variation in composition from within and between larger apparently single crystals is that the variation in analyses is due to inclusions or intimate intergrowths of other phases. Such inclusions would be more likely to occur in the larger crystals and aggregates of small crystals than in the smaller single crystals, which represent the great majority of these specimens. This explanation has no serious implications for the proposed formulae, $Sb^{III}Sb^{V}_{x}Nb_{1-x}TiO_6$ and $Sb^{III}Sb^{V}_{x}Ta_{1-x}TiO_6$, as the non-conforming analyses represented only a small proportion of the samples. These microanalytical data gave us sufficient confidence to use the simplest compositions $Sb_{1.0}A_{1.0}Ti_{1.0}$ (A = Nb, Ta) in our structure refinements described below.

3. XRD data collection

Data were collected using the powder diffractometer at the Australian National Beamline Facility, Photon Factory, Tsukuba, Japan.† Samples comprised finely ground powders mixed with Si (NBS standard 640b) as an internal standard loaded into 0.2 mm glass capillaries, which were rapidly spun during data collection. Two imaging plates were used to collect the powder diffraction data in Debye–Scherrer geometry from 5–45 and 45–85° 2θ, respectively. All measurements were performed under vacuum to minimize air scatter. The divergence of the beam in the direction of 2θ was 0.002 Å and the sample-to-imaging plate distance was 573 mm.

For the variable wavelength series on $Sb^{III}Sb^{V}_{x}Ta_{1-x}TiO_6$ a Weissenberg screen was used in combination with a translating imaging plate cassette to allow a number of exposures to be taken at different wavelengths using the same set of imaging plates. Each exposure yielded a strip 50 pixels wide which, when extracted and integrated, gave a powder profile with a step increment of 0.010044° in 2θ. Maximum peak heights were *ca* 105 counts with typical backgrounds of *ca* 103 counts.

The wavelengths chosen were 1.2618 (1), 1.2571 (1), 1.2566 (1), 1.2562 (1), 1.2557 (1), 1.2552 (1), 1.2547 (1), 1.2542 (1) and 1.2537 (1) Å for $Sb^{III}Sb^{V}_{x}Ta_{1-x}TiO_6$ and 1.2618 (1) Å for $Sb^{III}Sb^{V}_{x}Nb_{1-x}TiO_6$ calibrated from the internal Si standard. The wavelengths were selected to obtain data sets at different wavelengths approaching the Ta L_{III} absorption edge at λ = 1.255 Å to provide a range of scattering contrasts between the metal atoms in the $Sb^{III}Sb^{V}_{x}Ta_{1-x}TiO_6$ sample. Ultimately only data collected at λ = 1.2618 and 1.2547 Å were used for structure refinement.

4. Refinement of $Sb^{III}Sb^{V}_{x}Ta_{1-x}TiO_6$, λ = 1.2618 Å

The first refinement was carried out on what appeared to be the highest resolution data set; that of the Ta-containing compound at λ = 1.2618 Å, the wavelength furthest from the Ta L_{III} absorption edge.

The unit cell of $Sb^{III}Sb^{V}_{x}Ta_{1-x}TiO_6$ was determined from ED and refined using XRD (Guinier–Hägg camera) as monoclinic, a = 16.670 (5), b = 4.8171 (8), c = 5.489 (1) Å, β = 91.144 (1)°. This cell was used as the starting point in the refinement. The space-group symmetry of the proposed model was $C2/c$, in accordance with electron diffraction evidence (Ling, Thompson *et al.*, 1996). Anomalous dispersion coefficients at the appropriate wavelengths were calculated using the program *FPRIME* (Cromer & Liberman, 1981).

Refinement of the proposed model was carried out using *GSAS* (Larson & Von Dreele, 1991). For the 5–45° 2θ data set, a six-term cosine Fourier series background function, a scale factor, lattice parameters and three profile coefficients (Gaussian W, Cauchy Y and asymmetry) in the pseudo-Voigt function were refined. The same parameters were then refined for the 45–85° 2θ data set.

Metal-atom positions were then refined, converging rapidly without significant displacements from the starting model. O atoms behaved similarly on refinement. Isotropic thermal parameters were constrained to be equal for all sites and refined, however, the refinement always and immediately made this global thermal parameter negative. Constraining other refinement vari-

† The numbered intensity of each measured point on the profile has been deposited with the IUCr (Reference: AB0373). Copies may be obtained through The Managing Editor, International Union of Crystallography, 5 Abbey Square, Chester CH1 2HU, England.

ables demonstrated that this effect was not due to correlation. Superimposed plots of calculated *versus* observed profiles showed a clear trend of undercalculated intensities at low angle and overcalculated intensities at high angles, which the refinement compensated for with negative thermal parameters. The introduction of an arbitrary absorption factor placed the thermal parameters back on scale. The almost complete correlation between absorption and thermal parameters in the formulation used by *GSAS* has been recognized by Larson & Von Dreele (1991). Consequently, an arbitrary absorption factor was chosen which gave sensible thermal parameters on refinement. Once this correction had been applied, a stable refinement was obtained with anisotropic thermal parameters on metal atoms and isotropic thermal parameters on O atoms. Metals on the mixed site were constrained to have equal thermal parameters and all O atoms were constrained to have equal thermal parameters.

Finally, an attempt was made to refine the occupancy of the mixed metal site, constraining Ti occupancy to 0.5 and (Ta + Sb) occupancy to 0.5 (*i.e.* refining x). This refinement failed to converge and was abandoned. The data clearly did not possess the resolution to discriminate between the two metals, despite the enhanced scattering contrast for these metals due to the proximity of the Ta L^{III} absorption edge. Coarse compositional features, whereby Ti and Ta share one site while Sb^{III} occupies the other, could, however, be discriminated; a refinement cycle with a statistical distribution of metal-atom types

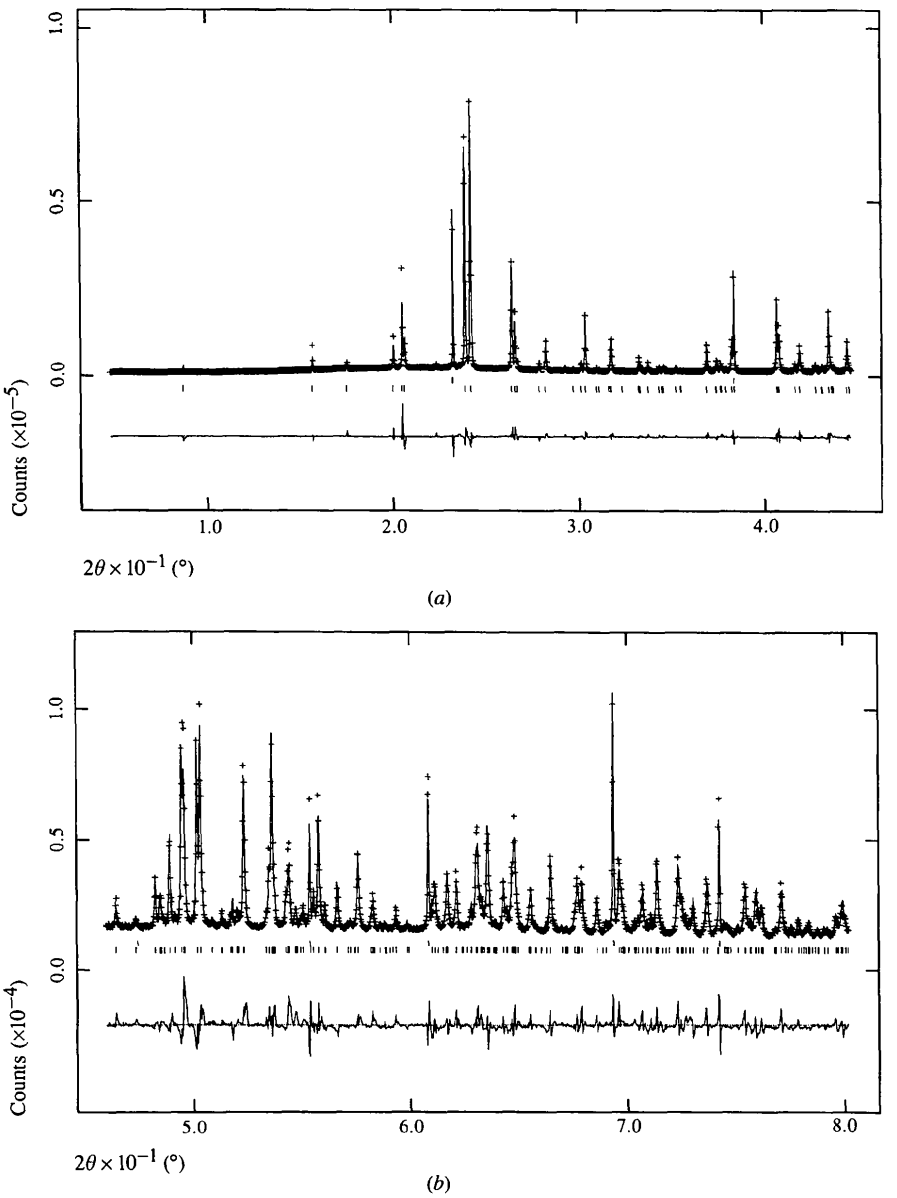

Fig. 2. Observed (crosses), calculated (solid line) and difference (below) XRD profiles of $Sb^{III}Sb^{V}_{x}Ta_{1-x}TiO_6$ at $\lambda = 1.2618$ Å. The bottom row of reflection markers represents the Si standard, the top row $Sb^{III}Sb^{V}_{x}Ta_{1-x}TiO_6$.

Table 1. *Experimental details*

	$Sb^{III}Sb^{V}_{x}Ta_{1-x}TiO_6$	$Sb^{III}Sb^{V}_{x}Nb_{1-x}TiO_6$
Crystal data		
Chemical formula weight	449.50	358.56
Cell setting	Monoclinic	Monoclinic
Space group	*C*2/*c*	*C*2/*c*
a (Å)	16.57244 (11)	16.6009 (2)
b (Å)	4.82608 (3)	4.82702 (6)
c (Å)	5.48949 (3)	5.49330 (6)
β (°)	91.1727 (5)	91.1159 (9)
V (Å^3)	438.957 (5)	440.110 (9)
μ (mm^{-1})	61.19	46.74
Temperature (K)	293	293
Specimen shape	Cylinder	Cylinder
Specimen size (mm)	20 × 0.2	20 × 0.2
Specimen colour	Yellow	Yellow
Data collection		
Radiation type	Synchrotron	Synchrotron
Wavelength (Å)	1.2618	1.2618
2θ range (°)	5–85	5–85
2θ increment (°)	0.010044	0.010044
Measurement device	Image plate	Image plate
Measurement method	Debye–Scherrer	Debye–Scherrer
Absorption correction	Empirical (*GSAS*; Larson & Von Dreele, 1991)	Empirical (*GSAS*; Larson & Von Dreele, 1991)
Refinement		
R_p	0.0525	0.0557
wR_p	0.0774	0.0853
χ^2	12.14	19.51
No. of reflections used	7374	7263
No. of parameters used	42	47
Computer program	*GSAS* (Larson & Von Dreele, 1991)	*GSAS* (Larson & Von Dreele, 1991)
Profile function	Pseudo-Voigt	Pseudo-Voigt

Table 2. *Final refined structural parameters for $Sb^{III}Sb^{V}_{x}Ta_{1-x}TiO_6$ and $Sb^{III}Sb^{V}_{x}Nb_{1-x}TiO_6$*

Space group *C*2/*c* (no. 15), *a* = 16.57244 (11), *b* = 4.82608 (3), *c* = 5.48949 (3) Å, β = 91.173 (1)°; $U_{eq} = (1/3)\Sigma_i\Sigma_j U^{ij} a_i^* a_j^* \mathbf{a}_i.\mathbf{a}_j$ (Å^2 × 10^{-2}).

	x (Å)	*y* (Å)	*z* (Å)	Type	Fraction	U_{eq}
Sb	0	0.7059 (3)	1/4	Sb	1.000	1.44 (12)
Ta	0.17318 (8)	0.2407 (3)	0.1698 (2)	Ta	1/2	0.92 (10)
Ti	0.17318 (8)	0.2407 (3)	0.1698 (2)	Ti	1/2	0.92 (10)
O1	0.0654 (5)	0.4170 (14)	0.0877 (14)	O	1.000	0.19 (14)
O2	0.2177 (5)	0.5649 (15)	0.3525 (13)	O	1.000	0.19 (14)
O3	0.1375 (5)	0.0556 (15)	0.4376 (14)	O	1.000	0.19 (14)

Space group *C*2/*c* (no. 15); *a* = 16.6009 (2), *b* = 4.82701 (6), *c* = 5.49329 (6) Å, β = 91.116 (1)°; $U_{eq} = (1/3)\Sigma_i\Sigma_j U^{ij} a_i^* a_j^* \mathbf{a}_i.\mathbf{a}_j$ (Å^2 × 10^{-2}).

	x (Å)	*y* (Å)	*z* (Å)	Type	Fraction	U_{eq}
Sb	0	0.7062 (3)	1/4	Sb	1.000	3.42 (17)
Nb	0.17359 (1)	0.2410 (4)	0.1715 (3)	Nb	1/2	0.22 (11)
Ti	0.17359 (1)	0.2410 (4)	0.1715 (3)	Ti	1/2	0.22 (11)
O1	0.0769 (5)	0.4090 (16)	0.1004 (16)	O	1.000	0.65 (16)
O2	0.2199 (5)	0.5585 (17)	0.3474 (19)	O	1.000	0.65 (16)
O3	0.1416 (5)	0.0500 (19)	0.4337 (18)	O	1.000	0.65 (16)

across both metal-atom sites converged, but with considerably worse statistics.

The isotropic thermal parameter of the Si atom in the Si internal standard was refined, profiles fitted in the same way as for $Sb^{III}Sb^{V}_{x}Ta_{1-x}TiO_6$ above and the phase fraction scale factor refined.

The final refinement of 42 variables using 7375 observations yielded the residuals $R_{wp} = \Sigma|y_{io} - y_{ic}|/\Sigma y_{io} = 0.0774$ and $R_p = \Sigma[w_i(y_{io} - y_{ic})^2/\Sigma w_i y_{io}^2]^{1/2} = 0.0525$. The final reduced $\chi^2 = (R_{wp}/R_p)^2$ was 12.14. The observed, calculated and difference profiles are illustrated in Fig. 2. The largest features in the difference profile

occur at the Si peaks, the profiles of which could not be accurately modelled due to the small number of data points comprising these extremely sharp peaks. The refinement is summarized in Table 1 and final structural parameters appear in Table 2.

5. Refinement of $Sb^{III}Sb^{V}_{x}Ta_{1-x}TiO_6$, $\lambda = 1.2547$ Å

As a further test, the above refinement was repeated with the data recorded closest to the Ta L_{III} absorption edge ($\lambda = 1.2547$ Å). The much greater absorption for this data set highlighted two amorphous peaks, at ~22.5 and ~25.0° 2θ, which it proved necessary to exclude from the refinement. Anomalous dispersion coefficients were recalculated for the new wavelength.

The refinement strategy was the same as above, this time using the refined structure as a starting model. The Si standard was dealt with as above. An arbitrary absorption correction was again applied to place the thermal parameters on a sensible scale, after which the refinement converged rapidly to a solution insignificantly different from the starting model. Attempts to refine x as above were again unsuccessful.

The final refinement of 42 variables using 6737 observations yielded the residuals $R_{wp} = 0.0156$ and $R_p = 0.0111$. The final reduced χ^2 was 1.121. The observed, calculated and difference profiles are illustrated in Fig. 3. The largest features in the difference profile again occur at the Si peaks. Although the residuals for this refinement ostensibly indicate a better result than

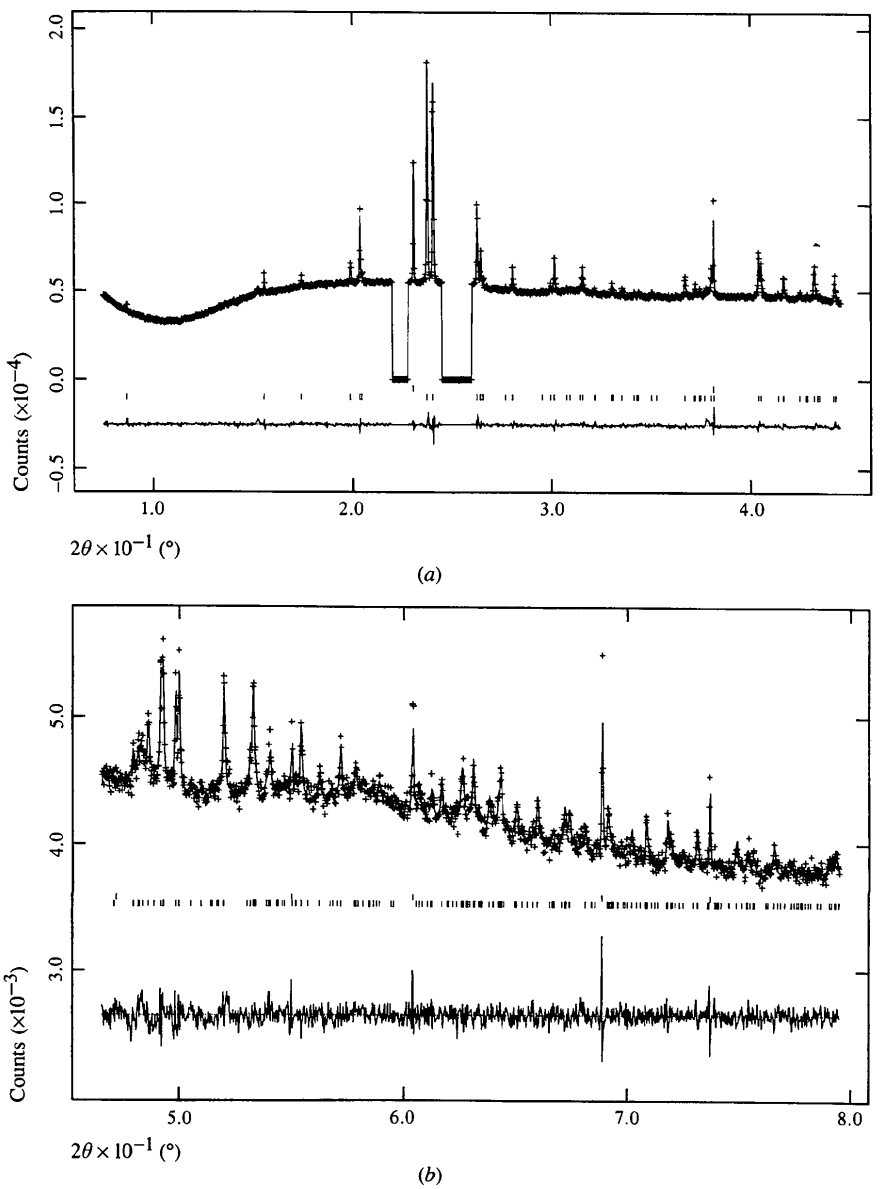

Fig. 3. Observed (crosses), calculated (solid line) and difference (below) XRD profiles of $Sb^{III}Sb^{V}_{x}Ta_{1-x}TiO_6$ at $\lambda = 1.2547$ Å. The bottom row of the reflection markers represents the Si standard, the top row $Sb^{III}Sb^{V}_{x}Ta_{1-x}TiO_6$.

obtained above, these are actually an artifact of the much lower peak-to-background ratio on the definitions of R_{wp}, R_p and χ^2. The accompanying loss of resolution leads to higher standard deviations in the parameters of the refined structure. Therefore, the solution obtained at the first wavelength is inherently more precise.

6. Refinement of $Sb^{III}Sb^{V}_{x}Nb_{1-x}TiO_6$, λ = 1.2618 Å

The unit cell of the starting model for $Sb^{III}Sb^{V}_{x}Nb_{1-x}TiO_6$ was determined from ED and refined using XRD (Guinier–Hägg camera) as monoclinic, a = 16.562 (2), b = 4.8318 (5), c = 5.4971 (5) Å, β = 91.190 (1)°. This cell was used as the starting point in the refinement. The space-group symmetry of the proposed model was $C2/c$, in accordance with electron diffraction evidence (Ling, Thompson *et al.*, 1996). As all the evidence indicated isomorphism between $Sb^{III}Sb^{V}_{x}Ta_{1-x}TiO_6$ and $Sb^{III}Sb^{V}_{x}Nb_{1-x}TiO_6$, the refined structure of the former was used as a starting model for refinement of the latter. Anomalous dispersion coefficients were calculated using *FPRIME* (Cromer & Liberman, 1981).

The refinement strategy followed that for $Sb^{III}Sb^{V}_{x}Ta_{1-x}TiO_6$ at the same wavelength. An arbitrary absorption correction was again necessary to put the thermal parameters on scale. Convergence was achieved without significant refinement of the starting parameters. It was not possible to refine metal-atom mixed occu-

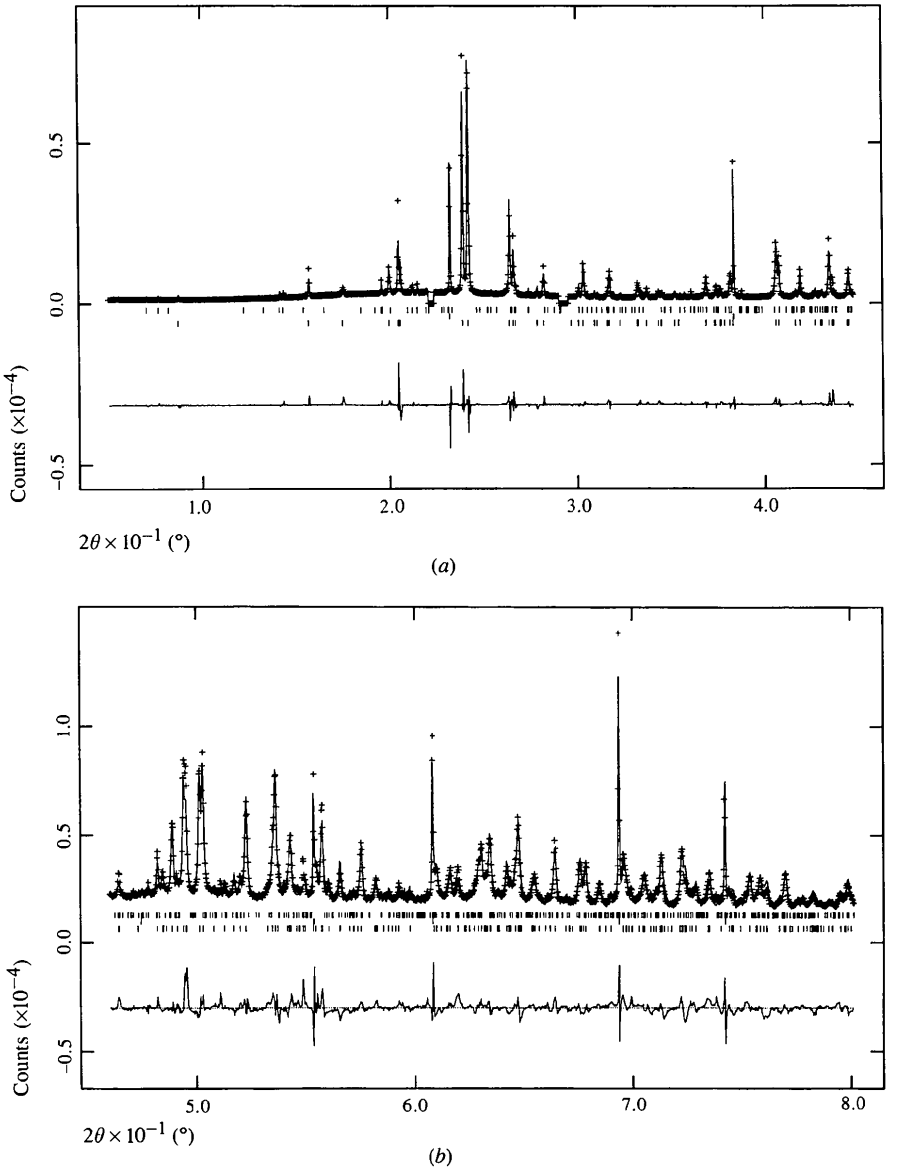

Fig. 4. Observed (crosses), calculated (solid line) and difference (below) XRD profiles of $Sb^{III}Sb^{V}_{x}Nb_{1-x}TiO_6$ at λ = 1.2618 Å. The bottom row of reflection markers represents $TiNb_2O_7$, the middle row the Si standard and the top row $Sb^{III}Sb^{V}_{x}Nb_{1-x}TiO_6$.

Table 3. *Bond-valence sums (Brese & O'Keefe, 1991) for possible metal atoms on the metal sites of the refined structures of* $Sb^{III}Sb^{V}_{x}A_{1-x}TiO_6$ *(A = Ta, Nb)*

		Sb^{III}	Sb^{V}	Ti^{IV}	Ta^{V}	Nb^{V}
A = Ta	Sb	3.196	2.939	2.085	2.703	—
	$Sb_xTa_{1/2-x}Ti_{1/2}$	5.828	5.359	3.802	4.929	—
A = Nb	Sb	2.314	2.128	1.460	—	1.957
	$Sb_xNb_{1/2-x}Ti_{1/2}$	6.568	6.040	4.285	—	5.554

pancies, although the coarse compositional features were reconfirmed as above by a random occupancy cycle.

In addition to the Si standard, dealt with as above, a further impurity was identified as $TiNb_2O_7$ (Gasperin, 1984). Gaussian *W*, Cauchy *Y* and asymmetry in the pseudo-Voigt function were refined for this phase, along with the unit cell and a phase-fraction scale factor, however, there were too few observations to refine atomic parameters. Two unexplained broad diffraction features, at ~22.5 and ~29.5° 2θ, were excluded from the refinement.

The final refinement of 47 variables using 7263 observations yielded the residuals R_{wp} = 0.0853 and R_p = 0.0557. The final reduced χ^2 was 19.51. The observed, calculated and difference profiles are illustrated in Fig. 4. The largest features in the difference profile again occur at the Si peaks. The refinement is summarized in Table 1 and final structural parameters appear in Table 2.

7. Discussion

Fig. 5 shows the refined structure of $Sb^{III}Sb^{V}_{x}A_{1-x}TiO_6$, *A* = Ta, *x* = 0, plotted by the program *CrystalMaker* (Palmer, 1994). The *A* = Nb structure is entirely analogous. The real structure is compared with a schematic polyhedral representation of the proposed *n* = 1 starting model (Ling, Thompson *et al.*, 1996). The real structure is derived from the idealized one by a small (~10°) rotation of the $Ta_{1/2}Ti_{1/2}O_6$ octahedra around axes parallel to **a**. This is the same relationship between the idealized and real structures of $Sb^{III}_3Sb^{V}_{x}A_{3-x}TiO_{14}$ (Ling, Schmid *et al.*, 1996), further evidence of the relationship between the two structures.

Both structures have been refined for the case *x* = 0, despite EDAX analyses indicating slightly above zero average values. The inability to refine *x* or distinguish between *x* = 0.0 and *x* = 0.1 (expected from the stoichiometry of the components) in $Sb^{III}Sb^{V}_{x}A_{1-x}TiO_6$ is not surprising given the very small differences in structure factors which this variation in composition represents. However, comparative refinement with models where the metals were distributed statistically over both metal sites gave a significantly poorer fit; at λ = 1.2618 Å, R_{wp} increased by 1.4% and R_p by 0.9% for Sb^{III} $Sb^{V}_{x}Ta_{1-x}TiO_6$, while R_{wp} increased by 1.01% and R_p by 0.5% for $Sb^{III}Sb^{V}_{x}Nb_{1-x}TiO_6$. These compositional features are supported by calculation of bond-valence sums for each metal-atom type in each site; Table 3 shows these values, which clearly indicate that the assumed metal-atom distribution is the only chemically plausible one.

Finally, although absorption effects mean that the refined atomic displacement parameters are not on an absolute scale, they still provide qualitative information about the structures. For the *A* = Ta case, reasonable

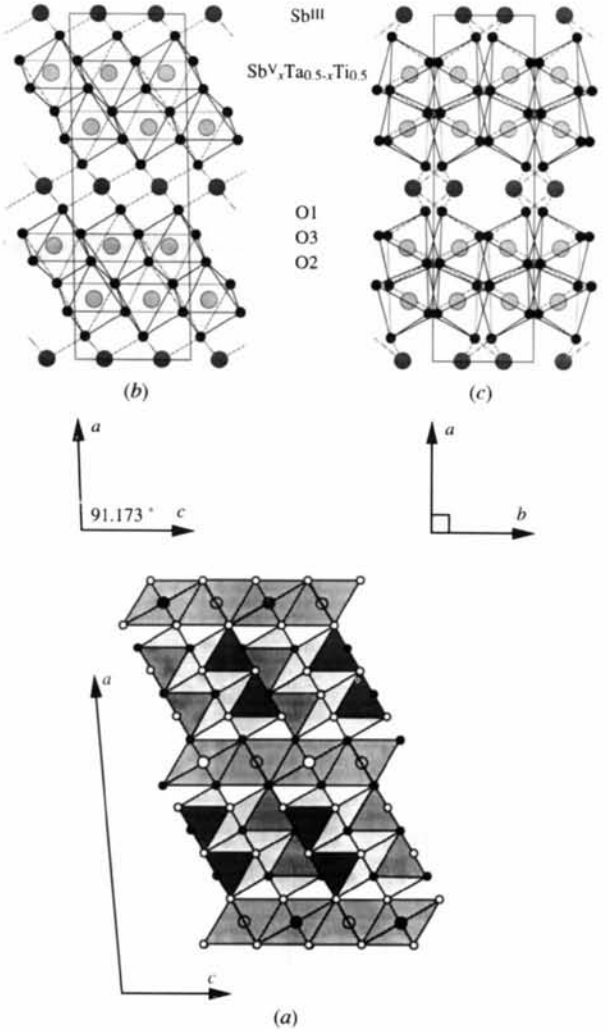

Fig. 5. The real structure of $Sb^{III}Sb^{V}_{x}Ta_{1-x}TiO_6$ projected along the (*a*) [010] and (*b*) [001] axes, compared with (*c*) a schematic polyhedral representation of the starting model projected along [010].

values were obtained. It is questionable whether the slightly anisotropic values for Sb are significant under the circumstances. For the A = Nb case, a stronger trend is observed towards Sb^{III} anisotropy in the U^{13} direction. This trend was also observed in the refined structures of $Sb_3^{III}Sb_x^{V}A_{3-x}TiO_{14}$ (A = Nb, Ta) and may therefore be explained in the same terms: as preferential motion of Sb^{III} along the Sb^{III}—O bonds. Anisotropy in the mixed metal site may be explained analogously.

All available evidence, therefore, supports the validity of the refined structures and the proposition that n = 1 and n = 3 members of the family $Sb_n^{III}Sb_x^{V}A_{n-x}TiO_{4n+2}$ are part of a structurally, as well as compositionally, homologous series.

References

Aurivillius, B. (1949). *Arkiv. Kemi*, **1**, 463–840.

Brese, N. E. & O'Keefe, M. (1991). *Acta Cryst.* B**47**, 192–197.

Cromer, D. T. & Liberman, D. A. (1981). *Acta Cryst.* A**37**, 267–268.

Gasperin, M. (1984). *J. Solid State Chem.* **53**, 144–147.

Hyde, B. G. & Andersson, S. (1989). *Inorganic Crystal Structures*, pp. 260–265. New York: Wiley.

Larson, A. C. & Von Dreele, R. B. (1991). *GSAS. The General Structure Analysis System.* Los Alamos National Laboratory.

Ling, C. D., Schmid, S., Thompson, J. G., Withers, R. L. & Sterns, M. (1996). *Acta Cryst.* B**52**, 932–938.

Ling, C. D., Thompson, J. G., Withers, R. L. & Schmid, S. (1996). *J. Solid State Chem.* **125**, 19–29.

Palmer, D. C. (1994). *CrystalMaker.* Lynxvale Ltd, Cambridge.